Supporting Information

Spatially Confined Proton-Coupled Electron Transfer in Functional Microcavities for Photocatalytic H_2O_2 Production in Pure Water

Yanzhuo Zhao, Xiaoya Li, Linghao Liu, Yuanying Liu, Yan Li, Xin Zhang, Hang Wang, Yichao Huang, Lin Wang* and Chuan-De Wu*

Shandong Key Laboratory of Intelligent Energy Materials, School of Materials Science and Engineering, China University of Petroleum (East China), Qingdao, P. R. China

*Corresponding author. Email: linwang@upc.edu.cn; cdwu@upc.edu.cn

Experimental Section

Materials

1,3,6,8-Tetrakis(4,4,5,5-tetramethyl-1,3,2-dioxaborolan-2-yl)pyrene (Py) was brought from Alpha Pharmaceutical Co., Ltd (Jiangsu, China). 2,5-Dibromopyrimidine, 3,6-dibromopyridazine and dimethyl 2,5-dibromoterephthalate were brought from Macklin Biochemical Co., Ltd (Shanghai, China). $Pd(PPh_3)_4$ was brought from Alfa Chemical Co., Ltd (Zhengzhou, China). Potassium carbonate was brought from Macklin Biochemical Co., Ltd (Shanghai, China). Commercial chemicals utilized in the experiment were employed without additional purification.

Synthesis of PyM

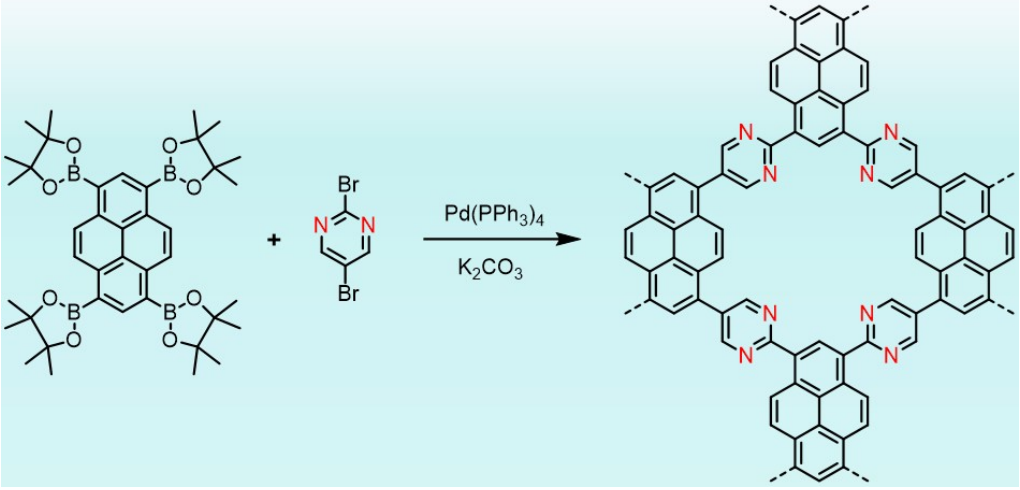

The synthesis of PyM was carried out in a 100 mL flask charged with a degassed mixture of DMF (50 mL) and deionized water (10 mL). The degassing was performed by N_2 bubbling for 30 minutes. Under a N_2 atmosphere, Py (0.2 mmol), 2,5-dibromopyrimidine (0.4 mmol), $Pd(PPh_3)_4$ (0.01 mmol) and K_2CO_3 (1 mmol) were introduced. The mixture was heated at 150 °C for 48 h. Upon cooling, the polymer was precipitated in a large volume of deionized water, isolated via filtration, and subjected to a sequential purification process: Soxhlet extraction with methanol (24 h) followed by dichloromethane (24 h). The product was finally dried under vacuum at 80 °C for 12 h to yield PyM.

Synthesis of PyD

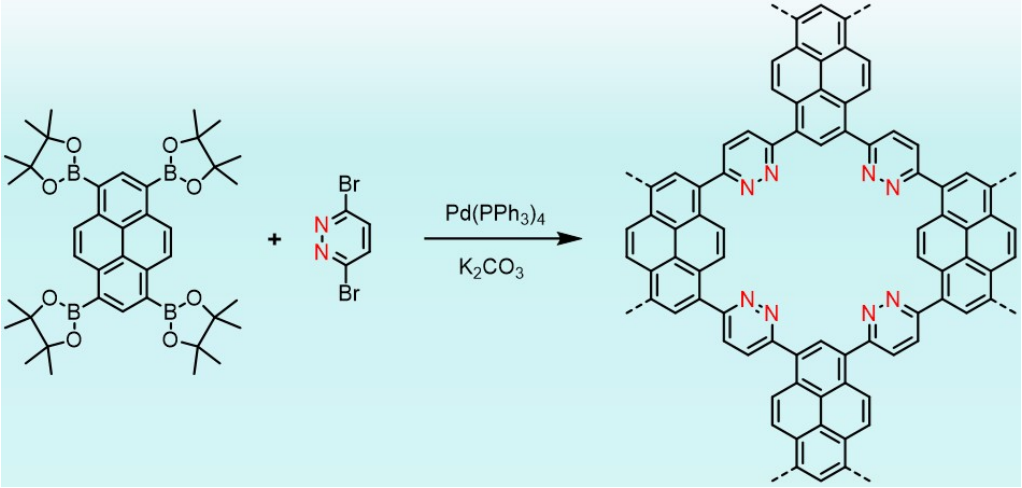

The synthesis of PyD was carried out in a 100 mL flask charged with a degassed mixture of DMF (50 mL) and deionized water (10 mL). The degassing was performed by N_2 bubbling for 30 minutes. Under a N_2 atmosphere, Py (0.2 mmol), 3,6-dibromopyridazine (0.4 mmol), $Pd(PPh_3)_4$ (0.01 mmol) and K_2CO_3 (1 mmol) were introduced. The mixture was heated at 150 °C for 48 h. Upon cooling, the polymer was precipitated in a large volume of deionized water, isolated via filtration, and subjected to a sequential purification process: Soxhlet extraction with methanol (24 h) followed by dichloromethane (24 h). The product was finally dried under vacuum at 80 °C for 12 h to yield PyD.

Synthesis of PyD-COOH

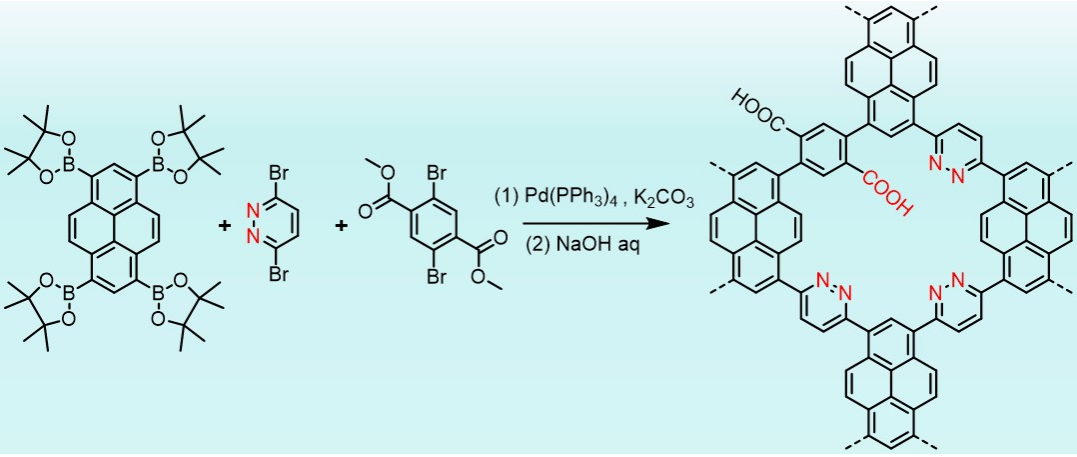

A mixture of DMF (50 mL) and deionized water (10 mL) in a 100 mL flask was

degassed by N_2 bubbling for 30 minutes. Under this inert atmosphere, Py (0.2 mmol), 3,6-dibromopyridazine (0.3 mmol), dimethyl 2,5-dibromoterephthalate (0.1 mmol), $Pd(PPh_3)_4$ (0.01 mmol) and K_2CO_3 (1 mmol) were added. The polymerization was conducted at 150 °C for 48 h. The crude polymer, isolated via precipitation in deionized water and filtration, underwent base hydrolysis (5 M NaOH, 80 °C, 12 h) to convert the ester groups to carboxylates. After washing, the material was acidified in a 0.5 M HCl solution (room temperature, 12 h) to yield the free carboxylic acid (–COOH) form, followed by extensive water washing. Purification was completed by successive Soxhlet extraction with methanol and dichloromethane (24 h each) and vacuum drying at 80 °C for 12 h, yielding the final polymer PyD-COOH.

Characterizations

Fourier transform infrared (FT-IR) spectra of the samples were recorded using a Shimadzu IRTracer-100 FT-IR spectrometer via the KBr pellet method. X-ray diffraction (XRD) patterns were collected on a Bruker D8 Advance powder X-ray diffractometer equipped with a Cu Kα radiation source (λ=1.5418 Å). X-ray photoelectron spectroscopy (XPS) measurements were performed using a Thermo Scientific ESCALAB 250Xi X-ray photoelectron spectrometer. Nitrogen adsorption-desorption isotherms were measured at 77 K on an Autosorb-iQ instrument, with samples degassed under vacuum at 120 °C for 12 hours prior to analysis. The specific surface areas of the samples were calculated using the Brunauer-Emmett-Teller (BET) method based on the nitrogen adsorption-desorption data. Scanning electron microscopy (SEM) images were acquired using a ZEISS Sigma 360 field-emission scanning electron microscope. Ultraviolet-visible diffuse reflectance spectroscopy (UV-Vis-DRS) was conducted with a UV-2007 spectrophotometer. All electrochemical measurements were carried out using a CHI 660E electrochemical workstation in a standard three-electrode system. Steady-state photoluminescence (PL) spectra were recorded on a Hitachi F-7000 spectrophotometer. The hydrophilicity and hydrophobicity of the catalysts were determined using a contact angle analyzer. Oxygen radicals ($\cdot O_2^-$) and hydroperoxyl radicals (·OOH) were detected by electron

paramagnetic resonance (EPR) spectroscopy using an EPR200M instrument.

Photocatalytic H_2O_2 measurements

1 mg of photocatalyst was dispersed in 30 mL deionized water and transferred into the reactor. Oxygen was then bubbled through the suspension for 30 min to ensure complete saturation. The reactor was subsequently sealed to maintain an oxygen-rich atmosphere. Photocatalytic reactions were carried out under irradiation from a 300 W Xe lamp equipped with a 400 nm cut-off filter. The reaction temperature was maintained at 25 °C using a circulating water cooling system with continuous magnetic stirring. At specified time intervals, 4 mL solution was taken with a syringe and filtered through a 0.2 μm filter to remove the photocatalyst. The filtrate was tested via UV–Vis spectroscopy to determine the H_2O_2 yield. H_2O_2 was quantified by the $Ce(SO_4)_2$ method using a UV-Vis spectrophotometer. The yellow Ce^{4+} is reduced by H_2O_2 to colorless Ce^{3+}, and Ce^{3+} shows strong absorption around 316 nm. A 1 mM $Ce(SO_4)_2$ solution (100 mL) was prepared in 0.5 M sulfuric acid. For the calibration curve, 1.75 mL of H_2O_2 with known concentrations was mixed with 1.75 mL of 1 mM $Ce(SO_4)_2$, and the UV-Vis measurement was done to get the linear relationship between H_2O_2 concentration and absorbance as follows.

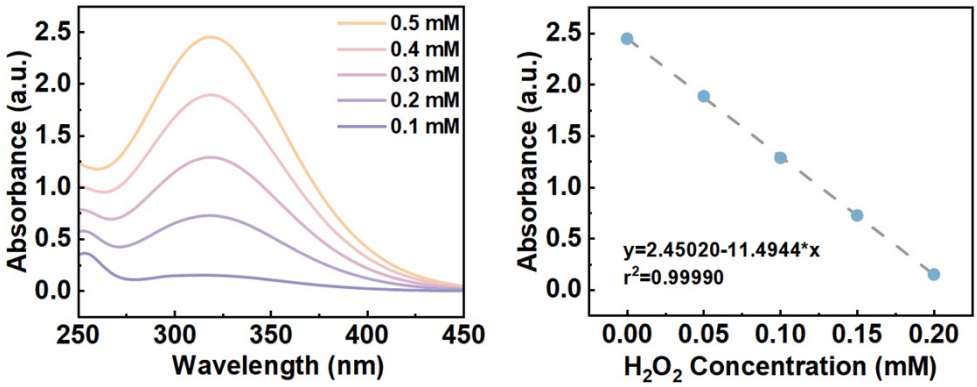

SCC efficiency (%) measurement

The solar-to-chemical energy conversion (SCC) efficiency was determined from photocatalytic experiments using an AM 1.5G spectrum as the light source (120 mW

cm^{-2}) with an irradiation duration of 1 hour, while the reaction temperature was maintained at 25 ℃. The SCC efficiency was calculated using the following equation:

$$SCC(\%) = \frac{\Delta G_{H_2O_2} \times n_{H_2O_2}}{E_{total} \times n_{H_2O_2}} \times 100 = \frac{\Delta G_{H_2O_2} \times n_{H_2O_2}}{ISt} \times 100$$

In the equation, ΔG is the free energy for hydrogen peroxide formation (117 kJ mol^{-1}); n is the amount of hydrogen peroxide produced; I is the light power intensity (120 mW cm^{-2}); S is the irradiated sample area (10.18 cm^2); t is the irradiation time (3600 s).

Photoelectrochemical Characterizations

Photoelectrochemical measurements were performed using a CHI 660E electrochemical workstation in a quartz electrolytic cell with a three-electrode system. A 300 W Xe lamp equipped with a 400 nm cut-off filter served as the light source. The working electrode was FTO glass coated with the sample, with an effective area of 1 cm^2. An Ag/AgCl electrode was used as the reference electrode, and a Pt sheet as the counter electrode. The electrolyte solution was 0.25 M Na_2SO_4. For working electrode preparation: 3 mg of photocatalyst powder was dispersed in 200 μL of anhydrous ethanol and sonicated for 30 minutes. Then, 18 μL of Nafion solution was added, followed by further sonication for 1 hour to ensure uniform dispersion. 20 μL of the suspension was dropped onto the FTO glass surface, and this process was repeated three times with uniform coating. The electrode was finally air-dried. Mott-Schottky (M-S) measurements were conducted at three frequencies: 500 Hz, 1000 Hz, and 1500 Hz. Electrochemical impedance spectroscopy (EIS) was performed over a frequency range of 0.01-100000 Hz. A 300 W xenon lamp served as the light source, and transient photocurrent was measured as a function of time under alternating light on/off cycles.

Rotating disk electrode (RDE) measurements

A mixture was prepared by adding 1 mL of ethanol and 10 μL of Nafion solution (5 wt %) to 10 mg of the catalyst, followed by ultrasonic treatment for 30 minutes to achieve uniform dispersion. Subsequently, 20 μL of the resulting suspension was

precisely pipetted and deposited onto the center of the disk electrode. The electrode was then allowed to dry at room temperature until complete evaporation of the solvent was achieved. The experiment was conducted using a three-electrode configuration: a RDE served as the working electrode, a saturated calomel electrode as the reference electrode, and a graphite rod as the counter electrode. The electrolyte employed was a 0.1 M phosphate buffer solution (pH=7), which was pre-saturated with oxygen by bubbling O_2 through it for 30 minutes prior to measurements. Linear sweep voltammetry was performed at ambient temperature with the electrode operating at various rotation speeds, yielding the corresponding voltammograms. The average electron transfer number was calculated using the Koutecky-Levich equation:

$$\frac{1}{J} = \frac{1}{J_L} + \frac{1}{J_K} = \frac{1}{B\omega^{1/2}} + \frac{1}{J_K}$$

$$B = 0.62nFC_0D_0^{2/3}v^{-1/6}$$

where J is the current density; J_K is the kinetic current densities; J_L is the diffusion-limiting current density; ω is the rotating speed (rpm); n is the transferred electron number; F is the Faraday constant (96485 C mol^{-1}); C_0 is the bulk concentration of O_2 (1.20×10^{-3} mol L^{-1}); D_0 is the diffusion coefficient of O_2 (1.9×10^{-5} cm^2 s^{-1}); ν is the kinetic viscosity of the electrolyte (0.01 cm^2 s^{-1}).

Proton Conductivity Test

Alternating current impedance measurements were performed using a CHI 660E electrochemical workstation over a frequency range of 0.1 Hz to 100,000 Hz, under conditions of 90% relative humidity and temperatures ranging from 313 K to 343 K. The proton conductivity was calculated via the following equation:

$$\sigma = \frac{L}{R \times S}$$

Where σ is the conductivity (S cm^{-1}); L is the sample thickness (cm); S is the cross-sectional area of the electrode (cm^2); R is the measured resistance (Ω).

Description of DFT Algorithm

All calculations were performed using density functional theory (DFT) as implemented in the Vienna Ab initio Simulation Package (VASP). The exchange-correlation potential was described within the generalized gradient approximation using the Perdew-Burke-Ernzerhof (PBE) functional (GGA-PBE). The projector augmented-wave (PAW) method was employed to treat interactions between ion cores and valence electrons. The plane-wave cutoff energy was fixed to 500 eV. Given structural models were relaxed until the Hellmann–Feynman forces smaller than -0.02 eV/Å and the change in energy smaller than 10^{-5} eV was attained. The vacuum thickness was set to be 25 Å to minimize interlayer interactions. During the relaxation, the Brillouin zone was represented by a Γ centered k-point grid of 1×1×1. Grimme's DFT-D3 methodology was used to describe the dispersion interactions among all the atoms in adsorption models.

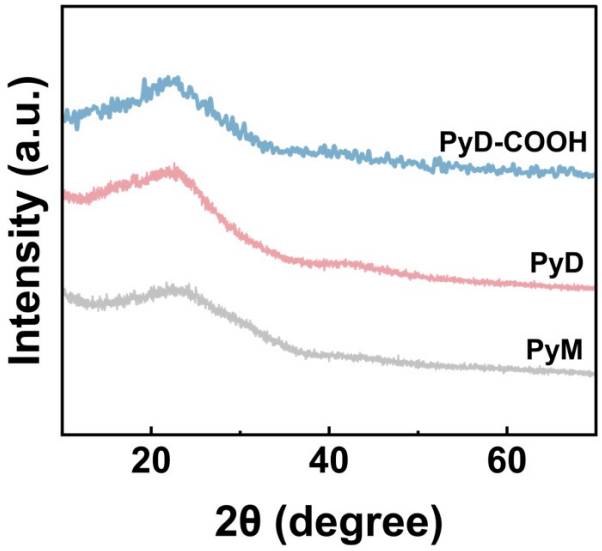

Figure S1. Powder XRD of PyM, PyD and PyD-COOH.

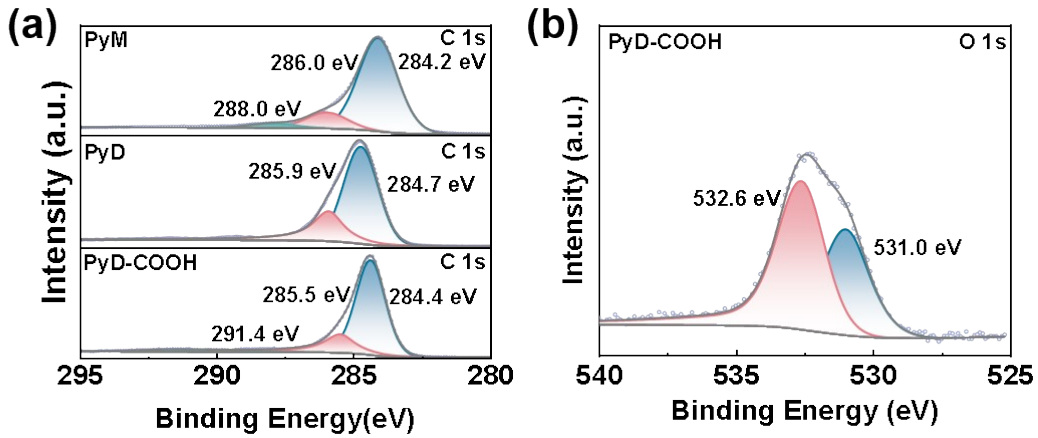

Figure S2. (a) XPS C 1s spectra of PyM, PyD and PyD-COOH. (b) XPS O 1s spectra of PyD-COOH.

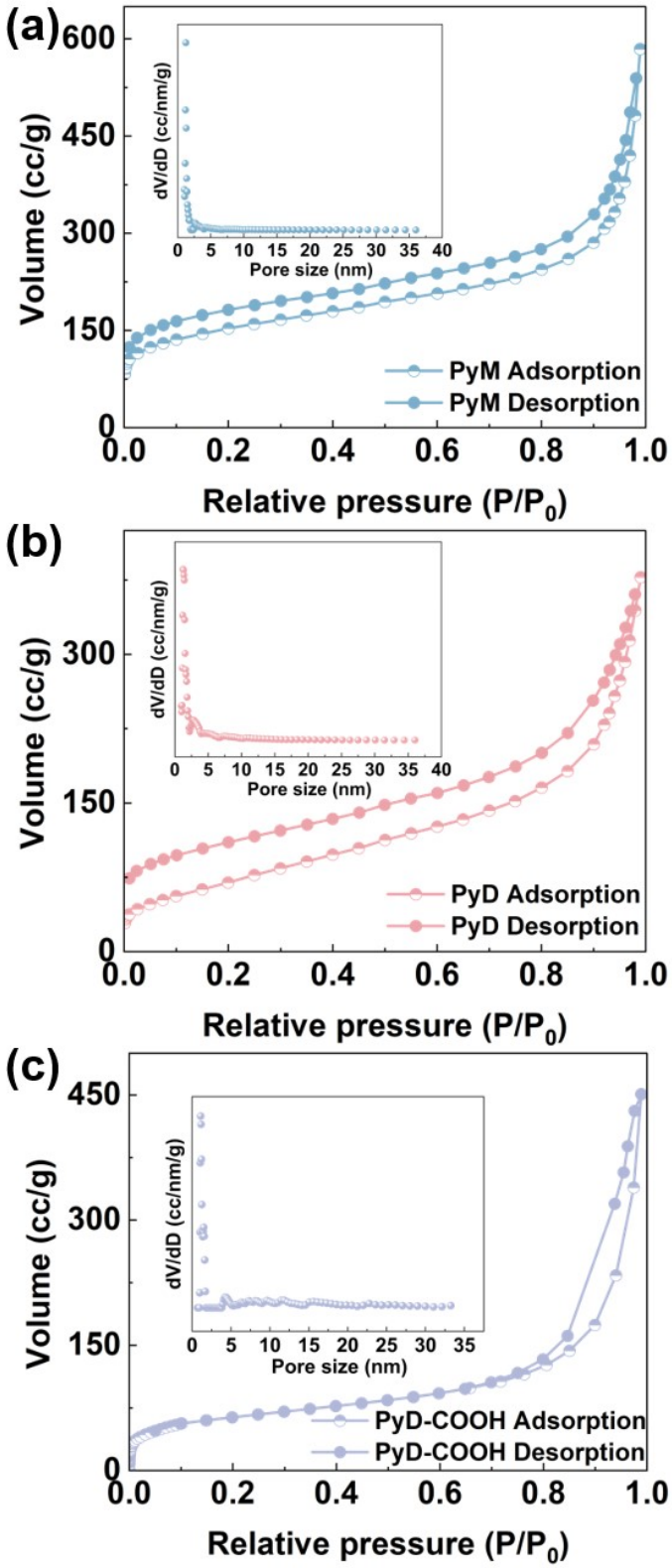

Figure S3. N_2 adsorption-desorption isotherms at 77.3 K and pore size distribution of (a) PyM, (b) PyD and (c) PyD-COOH.

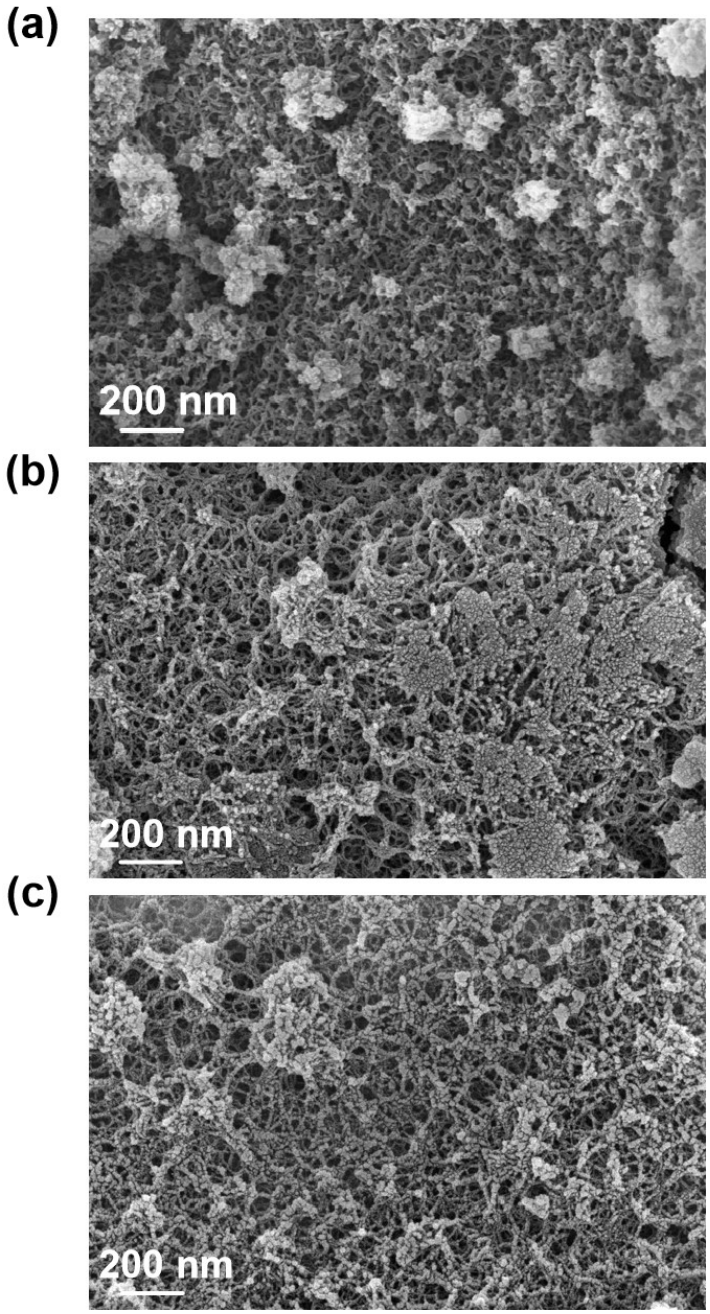

Figure S4. SEM images of (a) PyM, (b) PyD and (c) PyD-COOH.

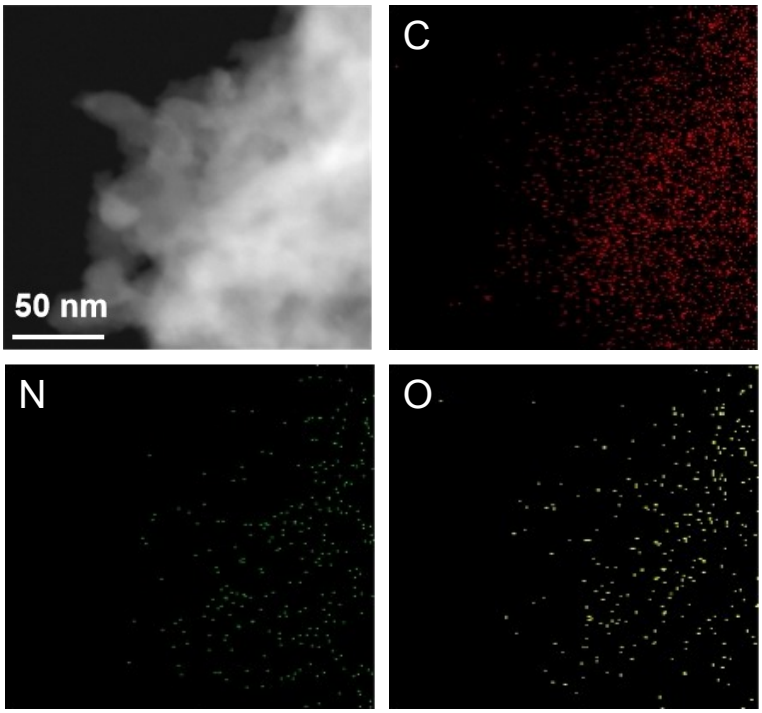

Figure S5. STEM image of PyD-COOH with corresponding elemental mappings for C, N and O.

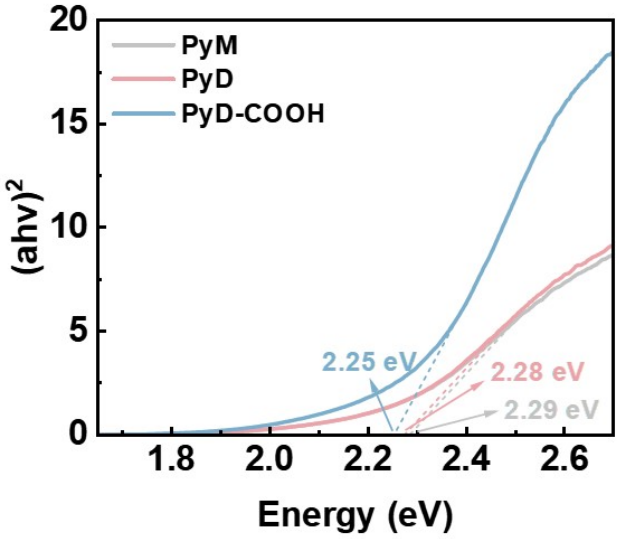

Figure S6. Tauc plot of PyM, PyD and PyD- COOH.

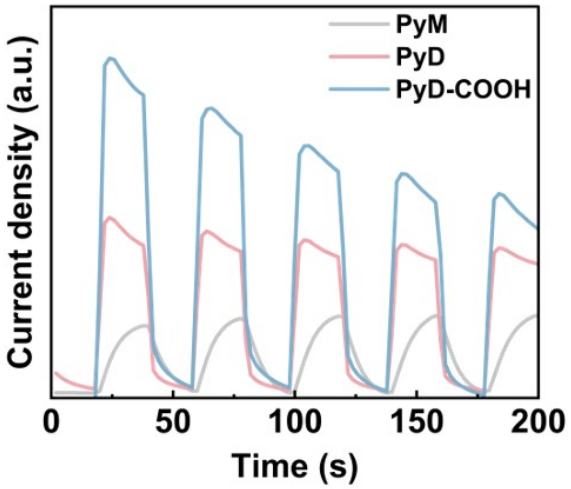

Figure S7. Photocurrent of PyM, PyD and PyD-COOH.

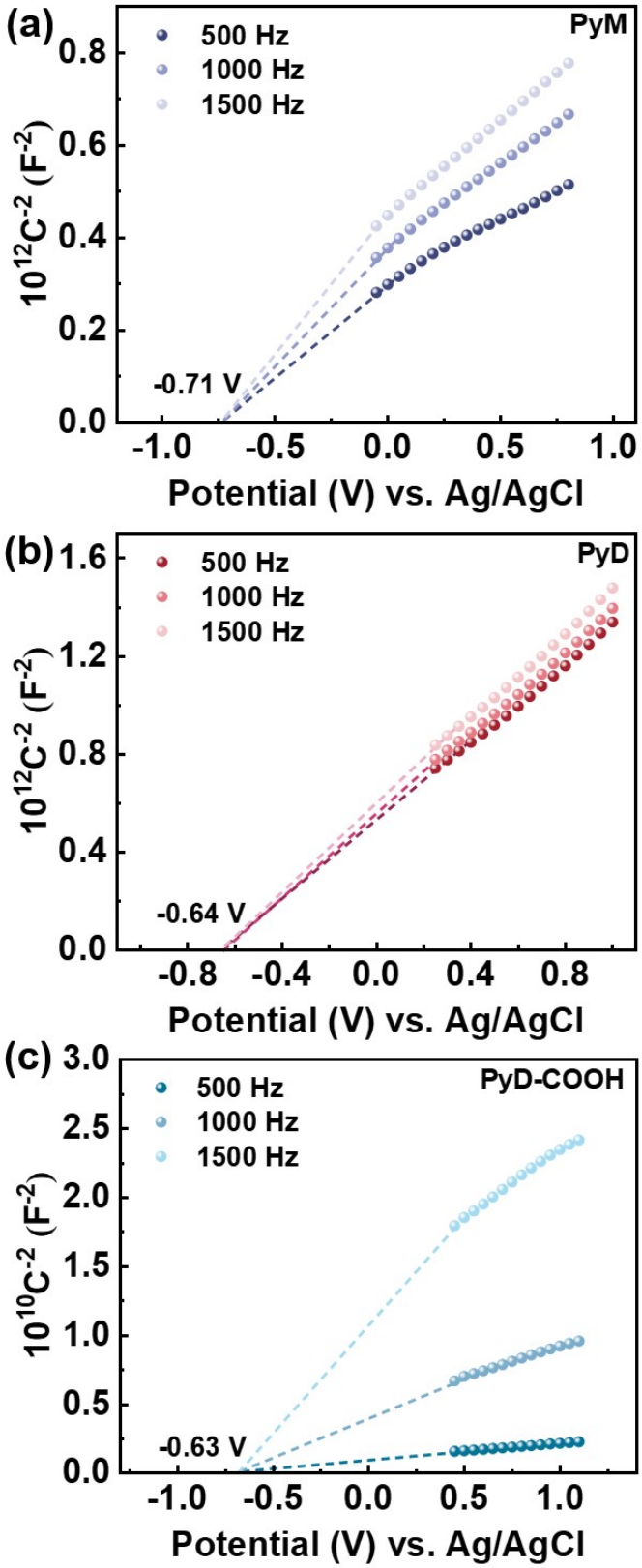

Figure S8. The Mott-Schottky plots of (a) PyM, (b) PyD and (c) PyD-COOH.

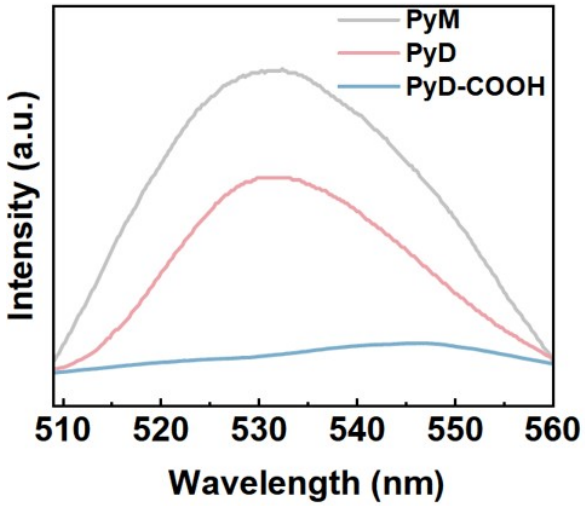

Figure S9. PL decay curves of PyM, PyD and PyD-COOH.

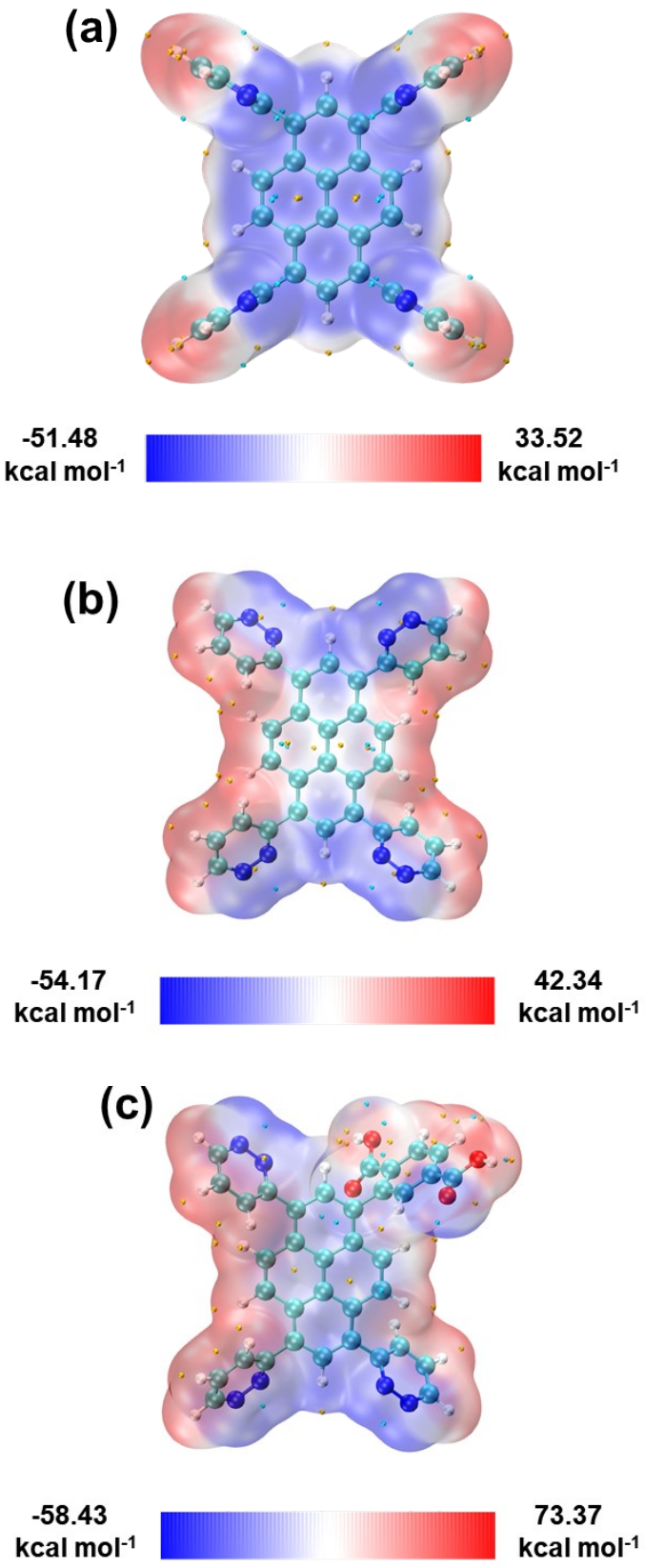

Figure S10. The electrostatic potential of (a) PyM, (b) PyD and (c) PyD-COOH.

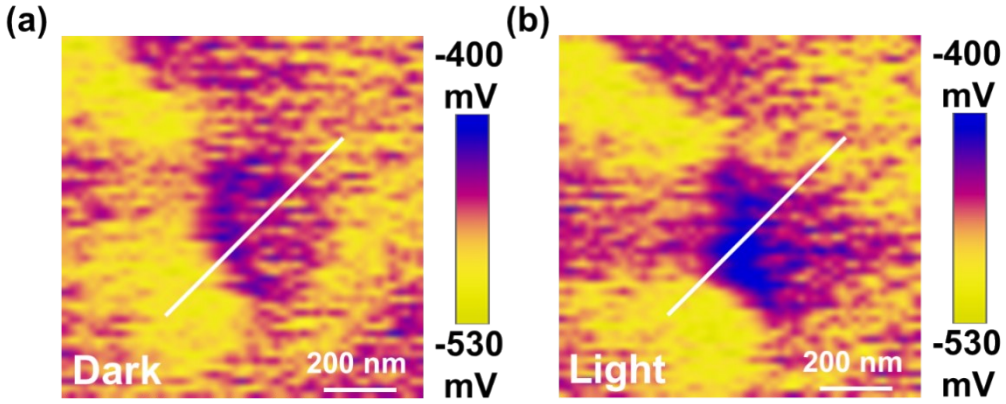

Figure S11. Surface potential before and after irradiation of PyM.

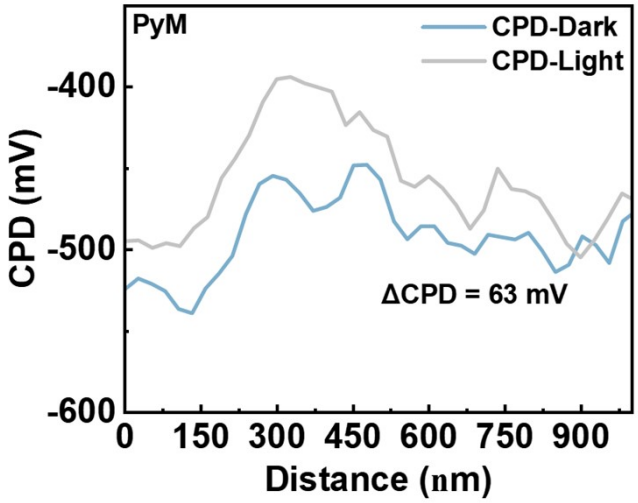

Figure S12. CPD curves before and after irradiation of PyM.

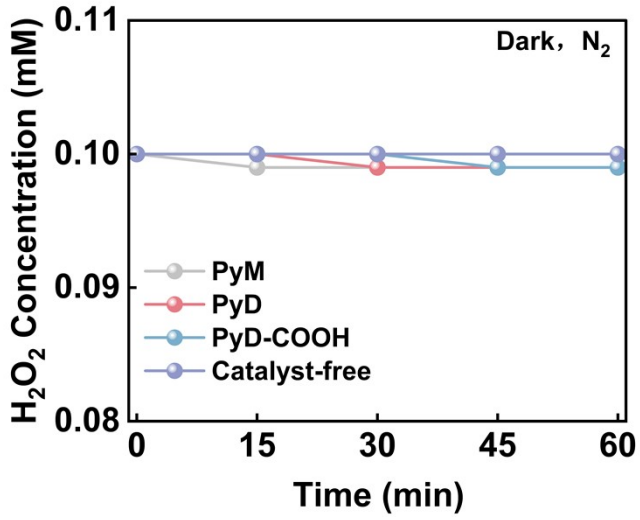

Figure S13. H_2O_2 concentration as a function of time.

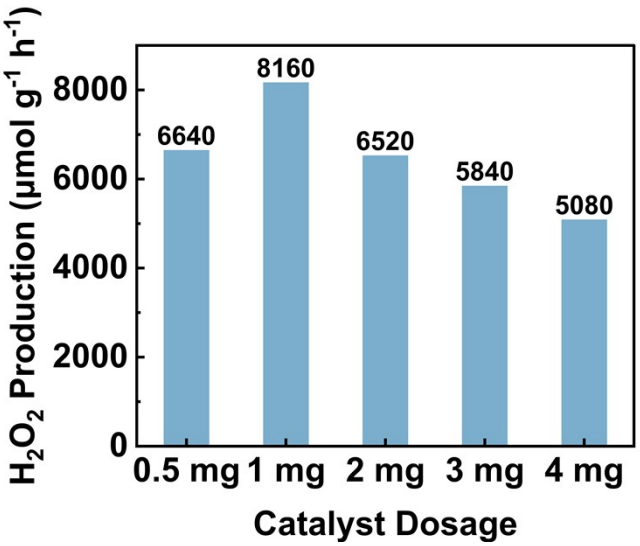

Figure S14. Dependence of H_2O_2 production on catalyst loading and irradiation time for PyD-COOH.

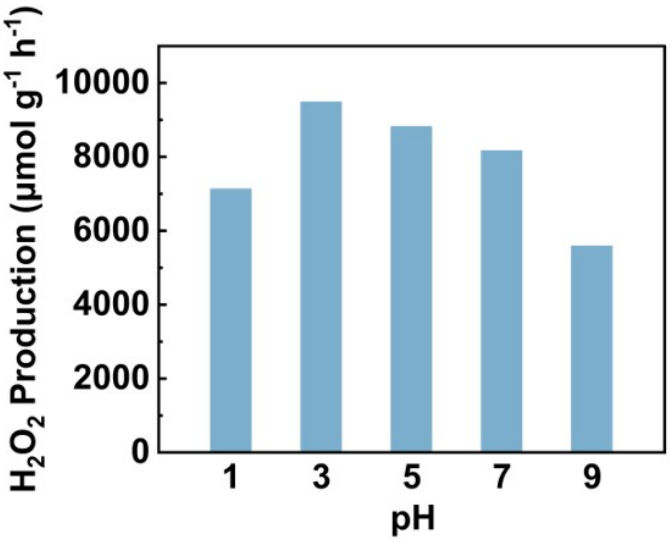

Figure S15. Photocatalytic H_2O_2 production of PyD-COOH at different pH values.

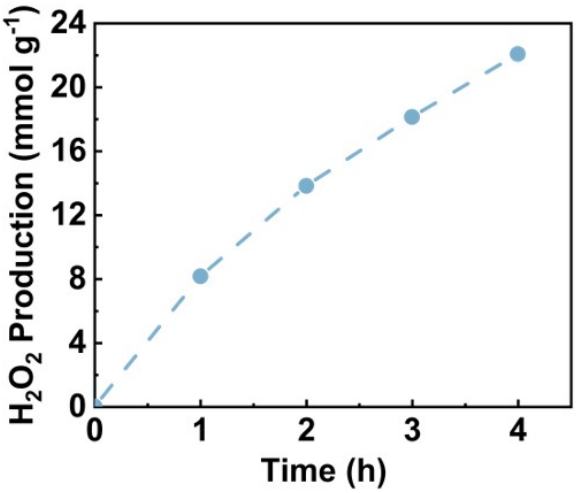

Figure S16. The variation of photocatalytic H_2O_2 production of PyD-COOH with reaction time.

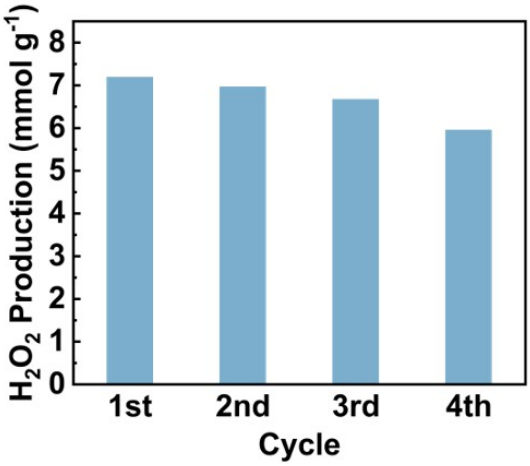

Figure S17. Recycling experiments for photocatalytic H_2O_2 production using PyD-COOH.

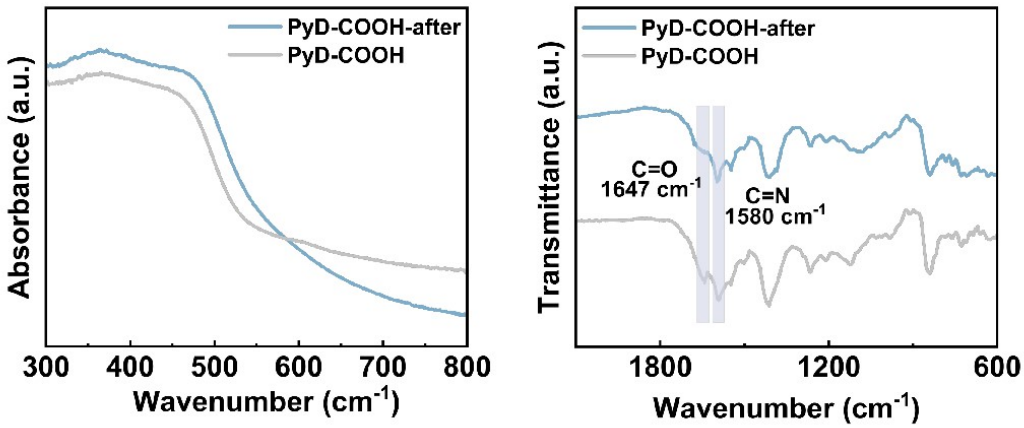

Figure S18. The UV-Vis diffuse reflectance absorption and FT-IR spectra of PyD-COOH before and after photocatalysis.

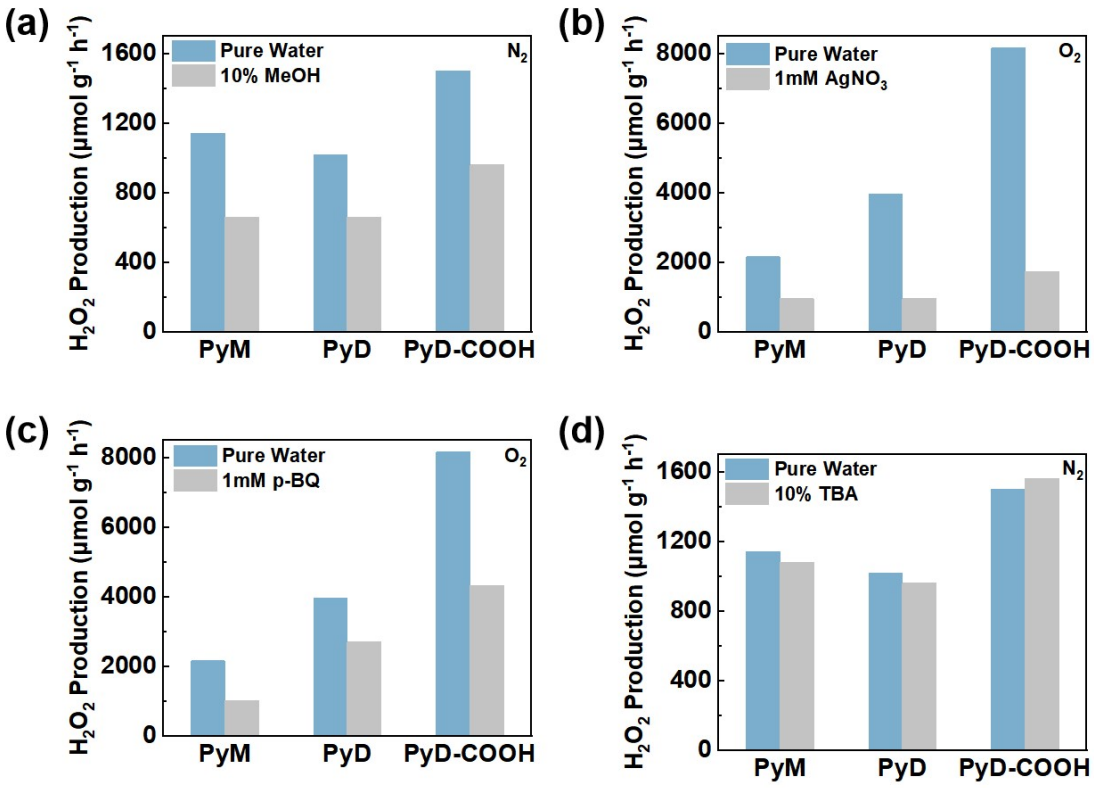

Figure S19. The Photocatalytic H_2O_2 production of three CPs (a) in pure water and 10% MeOH solution under N_2 atmosphere, (b) in pure water and 1 mM $AgNO_3$ solution under O_2 atmosphere, (c) in pure water and 0.1 mM p-BQ solution under O_2 atmosphere and (d) in pure water and 10% TBA solution under N_2 atmosphere.

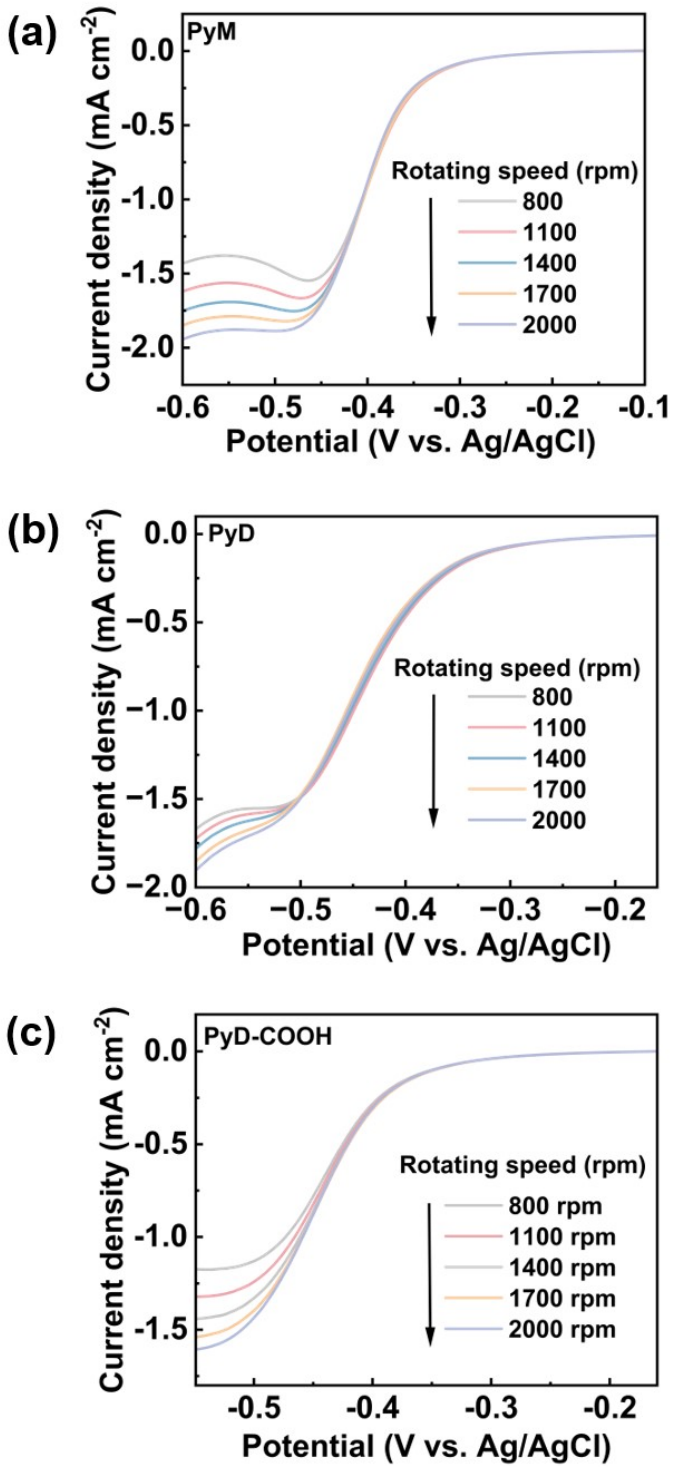

Figure S20. The LSV curves measured on RDE with different rotating rates of PyM, PyD and PyD-COOH.

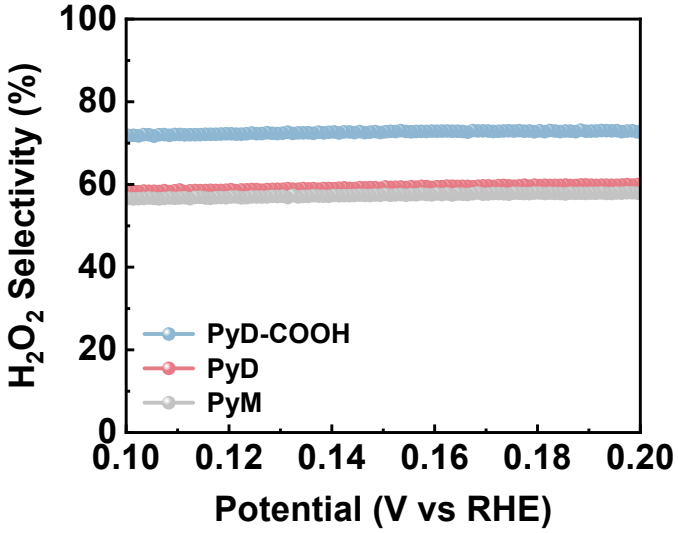

Figure S21. Electrochemical H_2O_2 selectivity of PyM, PyD and PyD-COOH in 0.1 M Na_2SO_4.

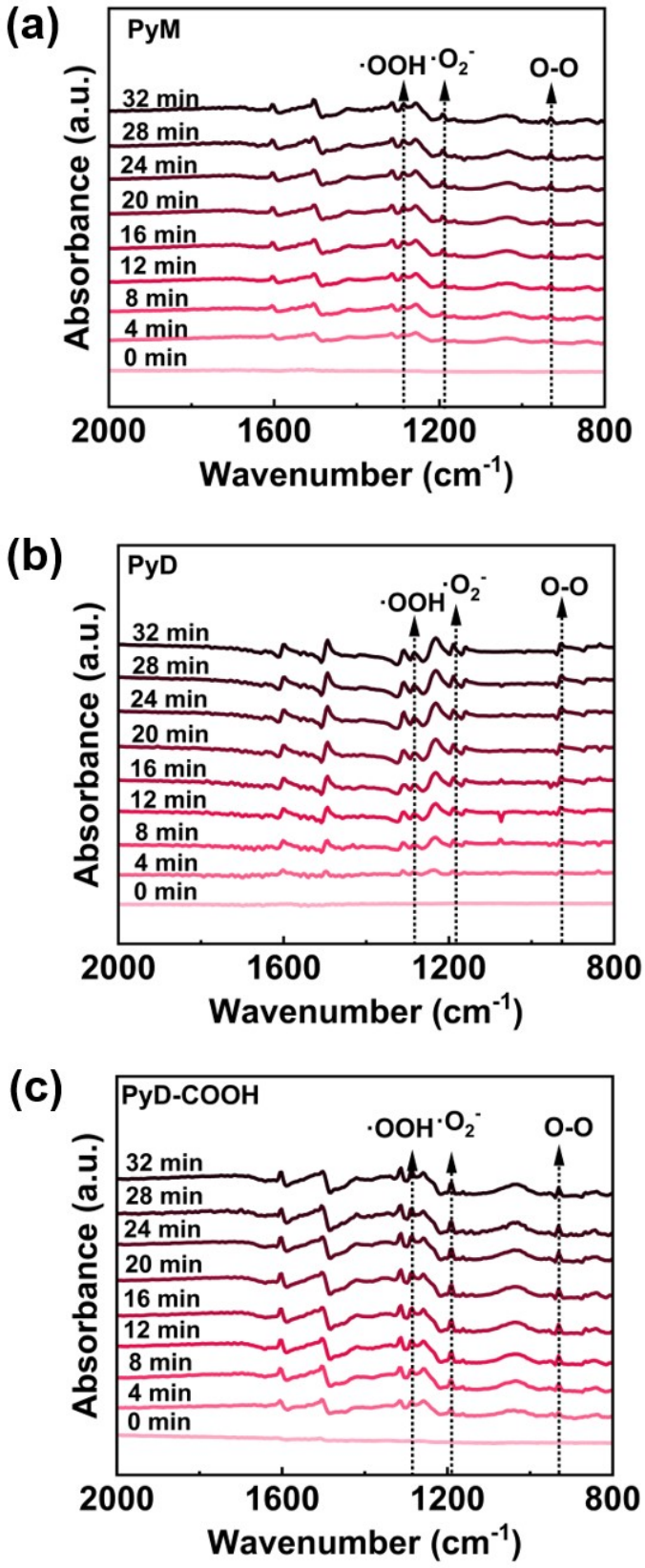

Figure S22. Time-dependent in situ attenuated total reflection-infrared (ATR-IR) spectroscopy for PyM, PyD and PyD-COOH.

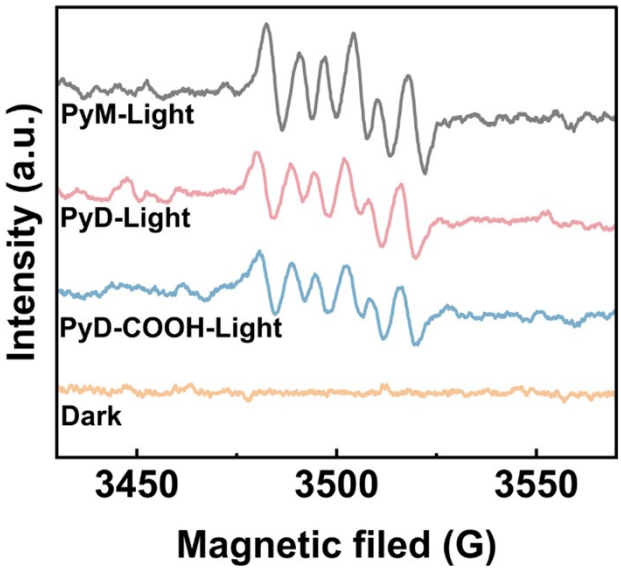

Figure S23. The EPR spectroscopy of PyM, PyD and PyD-COOH.

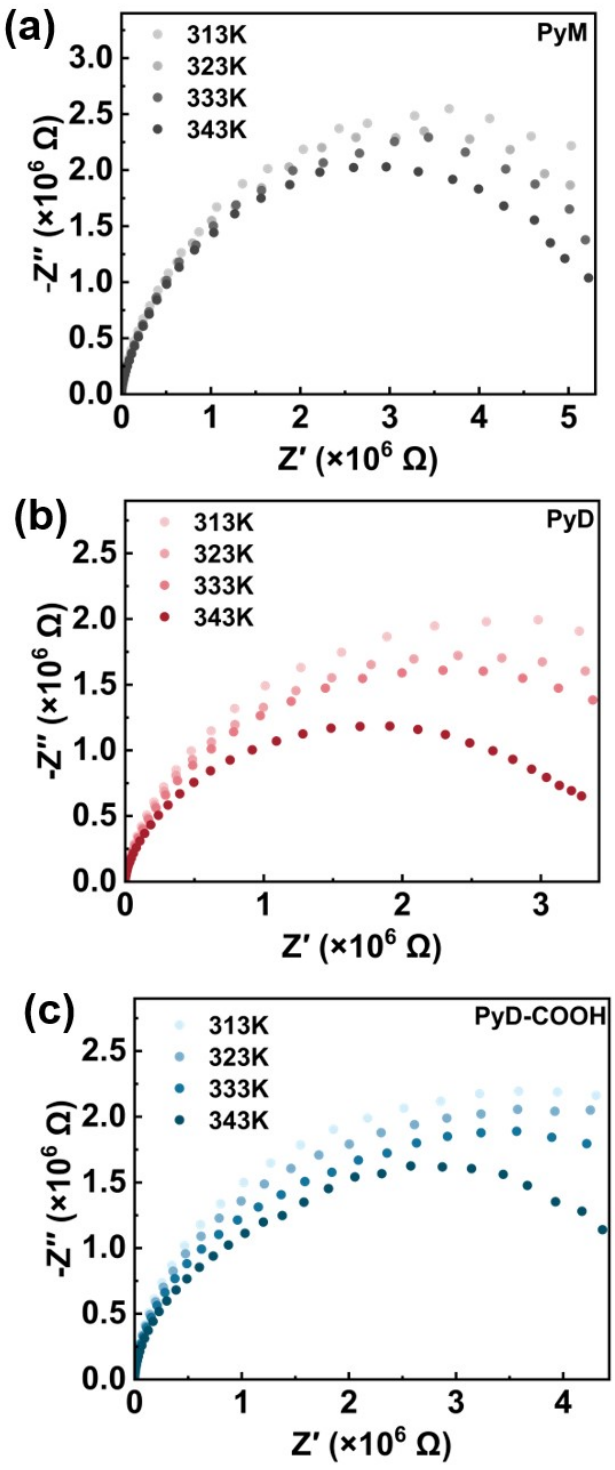

Figure S24. Nyquist plots of PyM, PyD, and PyD-COOH measured at temperatures ranging from 313 to 343 K under 90% RH.

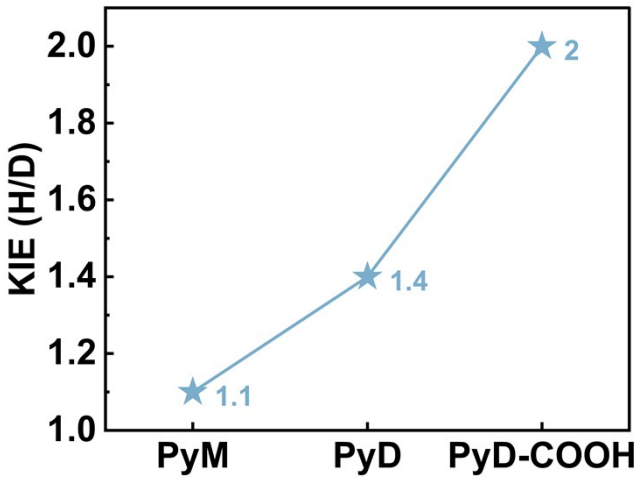

Figure S25. KIE of H/D of PyM, PyD and PyD-COOH.

Table S1. The dipole moment of PyM, PyD and PyD-COOH.

Samples	Dipole moment (Debye)
PyM	0.011
PyD	0.034
PyD-COOH	7.584

Table S2. Comparison of H_2O_2 production rate of PyD-COOH with previous reports.

Samples	Light	Condition	SCC	H_2O_2 yield ($\mu mol\ g^{-1}\ h^{-1}$)	Ref
PyD-COOH	**≥ 400 nm**	**H_2O, O_2**	**0.41%**	**8160**	**This work**
Py-Da-COF	≥ 420 nm	H_2O, O_2	0.09%	461	1
TT-T-COF	≥ 420 nm	H_2O, O_2	-	596	2
PMCR-1	420-700 nm	H_2O, O_2	-	1445	3
HITMS-COF-21H+	≥ 420 nm	H_2O, O_2	-	1957	4
Tp-TTz COF	-	H_2O, O_2	0.72%	2300	5
BBT-ACN COF-1	≥ 420 nm	H_2O, O_2	-	2500	6
BDP-AAQ	_	H_2O, O_2	0.61%	3000	7
oBPY-COF	≥ 420 nm	H_2O, O_2	0.59%	3638	8
g-COF-DMDP-1	≥ 420 nm	H_2O, O_2	-	3820	9
TTH–CTP	_	H_2O, O_2	-	4100	10
COF-JLU51	AM 1.5	H_2O, O_2	0.19%	4200	11
CZ-AQ	≥ 400 nm	H_2O, O_2	1.25%	4401	12
COF-C_4N	AM 1.5	H_2O, O_2	0.56%	4501	13
EBBT-COF	≥ 400 nm	H_2O, O_2	1.17%	5686	14
PTTN-AO	≥ 420 nm	H_2O, O_2	0.61%	6024	15
TpMaTAE	≥ 420 nm	H_2O, O_2	1.03%	6280	16
sp^3-SF-AQ	≥ 420 nm	H_2O, O_2	1.15%	6434	17
TpDz	≥ 420 nm	H_2O, O_2	0.62%	7327	18
CTF-BTT	≥ 420 nm	H_2O, O_2	0.66%	8099	19

References

1 J. Sun, H. Sekhar Jena, C. Krishnaraj, K. Singh Rawat, S. Abednatanzi, J. Chakraborty, A. Laemont, W. Liu, H. Chen, Y.-Y. Liu, K. Leus, H. Vrielinck, V. Van Speybroeck and P. Van Der Voort, *Angew. Chem., Int. Ed.*, 2023, **62**, e202216719.

2 J. Chen, S. Yan, F. Wang, F. Lin, J. Lin, R. A. Borse and Y. Wang, *Angew. Chem., Int. Ed.*, 2025, **64**, e202500924.

3 P. Das, J. Roeser and A. Thomas, *Angew. Chem., Int. Ed.*, 2023, **62**, e202304349.

4 L. Wang, C. Han, S. Gao, J.-X. Jiang and Y. Zhang, *ACS Catal.*, 2025, **15**, 5683-5693.

5 Z. Xue, B. Zhang, Q. Guo, Y. Wang, Q. Li, K. Yang and S. Qiao, *Adv. Mater.*, 2025, DOI: 10.1002/adma.202510201.

6 X. Wang, H. Li, S. Zhou, J. Ning, H. Wei, X. Li, S. Wang, L. Hao and D. Cao, *Adv. Funct. Mater.*, 2025, **35**, 2424035.

7 D. Wang, F. Tan, W. Zhao, S. Zhou, Q. Xu, L. Kan, L. Zhu, P. Gu and J. Lu, *Angew. Chem., Int. Ed.*, 2025, **64**, e202425017.

8 S. Liu, C. Zhu, H. Zhang, J. Wang, Q. Fang, C. Xu, S. Song and Y. Shen, *ACS Catal.*, 2025, DOI: 10.1021/acscatal.5c07226.

9 X. Chi, Z. Zhang, M. Li, Y. Jiao, X. Li, F. Meng, B. Xue, D. Wu and F. Zhang, *Angew. Chem., Int. Ed.*, 2025, **64**, e202418895.

10 S. Wang, Z. Xie, D. Zhu, S. Fu, Y. Wu, H. Yu, C. Lu, P. Zhou, M. Bonn, H. I. Wang, Q. Liao, H. Xu, X. Chen and C. Gu, *Nat. Commun.*, 2023, **14**, 6891.

11 Z. Zhang, Q. Zhang, Y. Hou, J. Li, S. Zhu, H. Xia, H. Yue and X. Liu, *Angew. Chem., Int. Ed.*, 2024, **63**, e202411546.

12 H. Yan, J. Jiang, Y. Huang, M. Shen, J. Xu, Y.-X. Ye and G. Ouyang, *Adv. Mater.*, 2026, **38**, e07961.

13 Y. Lai, Z.-D. Yang, G. Ren, W. Liu, Y. Liu, R. Cao, R. Zhang, G. Zhang and W. Zheng, *Adv. Funct. Mater.*, 2025, DOI: 10.1002/adfm.202515942.

14 B. Li, J. Chen, K. Wang, D. Qi, T. Wang and J. Jiang, *Advanced Energy Materials*, 2025, **15**, 2404497.

15 Z. Yu, F. Yu, M. Xu, S. Feng, J. Qiu and J. Hua, *Adv. Sci.*, 2025, **12**, 2415194.

16 G. Lv, X. Yu, J. Wang, J. Qiu, D. Yang and Y. Zhu, *Adv. Funct. Mater.*, 2025, DOI: 10.1002/adfm.202517393.

17 S. Zhu, X. He, L. Wang, W. Ma, C. Liu, Y. Zhang, X. Hu and J.-X. Jiang, *Adv. Funct. Mater.*, 2025, **n/a**, e19832.

18 Q. Liao, Q. Sun, H. Xu, Y. Wang, Y. Xu, Z. Li, J. Hu, D. Wang, H. Li and K. Xi, *Angew. Chem., Int. Ed.*, 2023, **62**, e202310556.

19 R. Sun, X. Yang, X. Hu, Y. Guo, Y. Zhang, C. Shu, X. Yang, H. Gao, X. Wang, I. Hussain and B. Tan, *Angew. Chem., Int. Ed.*, 2025, **64**, e202416350.